Supplemental Material for "Diversity of phase transitions and phase separations in active fluids"

Thibault Bertrand[1, *] and Chiu Fan Lee[2, †]

[1]*Department of Mathematics, Imperial College London,*
South Kensington Campus, London SW7 2AZ, United Kingdom
[2]*Department of Bioengineering, Imperial College London,*
South Kensington Campus, London SW7 2AZ, United Kingdom

I.   LINEAR STABILITY ANALYSIS

In this section, we proceed to the linear stability analysis of our hydrodynamic EOM in one dimension

$$\partial_t \rho + \partial_x p = \eta \partial_x^2 \rho \tag{1}$$

$$\partial_t p + \lambda p \partial_x p = \mu \partial_x^2 p - \kappa(\rho) \partial_x \rho + \alpha(\rho) p - \beta p^3 \tag{2}$$

A.   Instability of the homogeneous disordered state

First, we consider the stability conditions for the homogeneous disordered state, i.e. a state with zero average momentum density. We linearize Eqs. (1-2) around the homogeneous disordered state with $\rho = \rho_0 + \delta\rho$, $p = \delta p$, $\alpha(\rho) = -|\alpha_0|$ and $\kappa(\rho) = \kappa_0$. To linear order, we obtain

$$\partial_t \delta\rho = -\partial_x \delta p + \eta \partial_x^2 \delta\rho \tag{3}$$

$$\partial_t \delta p = \mu \partial_x^2 \delta p - \kappa_0 \partial_x \delta\rho - |\alpha_0| \delta p \tag{4}$$

with the fluctuation terms written as

$$\delta\rho = \delta\rho_0 \exp[st - \mathrm{i}kx] \tag{5}$$

$$\delta p = \delta p_0 \exp[st - \mathrm{i}kx] \tag{6}$$

Reinjecting the fluctuation terms in the linearized equations, one obtains

$$s\delta\rho_0 = \mathrm{i}k\delta p_0 - \eta k^2 \delta\rho_0 \tag{7}$$

$$s\delta p_0 = -k^2\mu\delta p_0 + \mathrm{i}k\kappa_0 \delta\rho_0 - |\alpha_0|\delta p_0 \tag{8}$$

which we can rewrite as the following eigenvalue problem

$$\mathbf{A}\delta\mathbf{u}_0 = s\delta\mathbf{u}_0 \ , \tag{9}$$

with $\delta\mathbf{u}_0 = (\delta\rho_0, \delta p_0)^\top$ and

$$\mathbf{A} = \begin{bmatrix} -k^2\eta & \mathrm{i}k \\ \mathrm{i}k\kappa_0 & -k^2\mu - |\alpha_0| \end{bmatrix} \tag{10}$$

We know that the stability conditions are given by the sign of $\mathrm{Re}[s]$; the eigenvalues of this 2×2 matrix are given by

$$s = \frac{\mathrm{Tr}\mathbf{A}}{2} \pm \frac{1}{2}\sqrt{(\mathrm{Tr}\mathbf{A})^2 - 4\det\mathbf{A}} \tag{11}$$

i.e.

$$s = -\frac{|\alpha_0| + k^2(\mu + \eta)}{2} \pm \frac{1}{2}\sqrt{[|\alpha_0| + k^2(\mu + \eta)]^2 - 4[|\alpha_0|\eta k^2 + \kappa_0 k^2 + \eta\mu k^4]} \tag{12}$$

---

* Electronic address: t.bertrand@imperial.ac.uk
† Electronic address: c.lee@imperial.ac.uk

We know that s is real as long as $\left[|\alpha_0| + k^2(\mu + \eta)\right]^2 - 4k^2\kappa_0 > 0 \iff |\alpha_0| \geq 0$ when $k \to 0$; which is true. In the hydrodynamic limit $(k \to 0)$, we can expand the square root and we obtain

$$s = -\frac{|\alpha_0| + k^2(\mu + \eta)}{2} \pm \frac{1}{2}\left[|\alpha_0|^2 - 2k^2(\mu + \eta)|\alpha_0| + (\mu + \eta)^2 k^4 - 4|\alpha_0|\eta k^2 - 4\kappa_0 k^2 - 4\eta\mu k^4\right]^{1/2} \tag{13}$$

$$\approx -\frac{|\alpha_0| + k^2(\mu + \eta)}{2} \pm \frac{1}{2}|\alpha_0|\left[1 - \frac{k^2(\mu + \eta)}{|\alpha_0|} - \frac{2\eta k^2}{|\alpha_0|} - \frac{2k^2\kappa_0}{|\alpha_0|^2}\right] \tag{14}$$

$$\approx -\frac{1}{2}\left[|\alpha_0| \pm |\alpha_0|\right] \pm \frac{\kappa_0}{|\alpha_0|}k^2 - \frac{1}{2}\left[(\mu + \eta)k^2 \pm (\mu + \eta)k^2\right] \pm \eta k^2 + \mathcal{O}(k^3) \tag{15}$$

Finally, this leads to the following two eigenvalues in the hydrodynamic limit

$$\boxed{s = \begin{cases} -|\alpha_0| + \left[\frac{\kappa_0}{|\alpha_0|} + \mu\right]k^2 + \mathcal{O}(k^3) \\ -\left[\frac{\kappa_0}{|\alpha_0|} + \eta\right]k^2 + \mathcal{O}(k^3) \end{cases}} \tag{16}$$

We interpret these solutions as follows:

- the first eigenvalue $-|\alpha_0|$ characterizes the *fast relaxation of the momentum fluctuations in the absence of spatial variations* $(k \to 0)$;

- the second eigenvalue $-k^2\left[\kappa_0/|\alpha_0| + \eta\right]$ controls the *onset of instability of the homogeneous disordered phase*.

We conclude that the homogeneous disordered phase is unstable when $\alpha(\rho) < 0$ and $\kappa(\rho) - \eta\alpha(\rho) < 0$ leading to phase separation and the emergence of the cD-dD phase co-existence (e.g. MIPS).

B. Stability of the homogeneous ordered phase

The results of the previous section hint at the fact that collective motion is expected in the case the momentum fluctuations do not relax quickly, i.e. when $\alpha(\rho) > 0$. Indeed, it is interesting to note that for a stable system $\beta > 0$ necessarily, thus $\alpha_0 > 0$ leads to collective motion, while $\alpha_0 \leq 0$ gives a stationary state. Naturally, the next step is thus to explore the stability of a homogeneous state displaying collective motion, i.e. a homogeneous ordered state. The steady-state homogeneous solutions are given by

$$\beta p^3 - \alpha_0 p = 0 \iff p_0 = 0 \text{ or } p_0 = \sqrt{\alpha_0/\beta} \tag{17}$$

Here, we thus expand about a homogeneous state displaying collective motion with

$$\begin{cases} \rho = \rho_0 + \delta\rho & = \rho_0 + \delta\rho_0 \exp[st - ikx], \\ p = p_0 + \delta p & = p_0 + \delta p_0 \exp[st - ikx], \\ \alpha = \alpha_0' + \alpha_1'\rho & = \alpha_0 + \alpha_1\delta\rho_0 \exp[st - ikx]. \end{cases} \tag{18}$$

with $p_0 = \sqrt{\alpha_0/\beta}$. To linear order, we obtain for the momentum equation

$$\begin{aligned} \partial_t\delta p + \lambda p_0\partial_x\delta p &= \mu\partial_x^2\delta p - \kappa\partial_x\delta\rho + (\alpha_0 + \alpha_1\delta\rho)(p_0 + \delta p) - \beta(p_0 + \delta p)^3 \\ &= \mu\partial_x^2\delta p - \kappa\partial_x\delta\rho + \alpha_0 p_0 + \alpha_1 p_0\delta\rho + \alpha_0\delta p - \beta(p_0^3 + 3p_0^2\delta p) \\ &= \mu\partial_x^2\delta p - \kappa\partial_x\delta\rho + \alpha_0 p_0 + \alpha_1 p_0\delta\rho + \alpha_0\delta p - \alpha_0 p_0 - 3\alpha_0\delta p \\ &= \mu\partial_x^2\delta p - \kappa\partial_x\delta\rho + \alpha_1 p_0\delta\rho + \alpha_0\delta p - 3\alpha_0\delta p \end{aligned}$$

The linearized equations of motion thus finally read

$$\partial_t\delta\rho = -\partial_x\delta p + \eta\partial_x^2\delta\rho \tag{19}$$

$$\partial_t\delta p + \lambda p_0\partial_x\delta p = \mu\partial_x^2\delta p - \kappa\partial_x\delta\rho + \alpha_1 p_0\delta\rho - 2\alpha_0\delta p \tag{20}$$

Reinjecting in these linearized equations the ansatz, we get

$$s\delta\rho_0 = ik\delta p_0 - k^2\eta\delta\rho_0 \tag{21}$$

$$s\delta p_0 - ik\lambda p_0\delta p_0 = -\mu k^2\delta p_0 + ik\kappa\delta\rho_0 + \alpha_1 p_0\delta\rho_0 - 2\alpha_0\delta p_0 \tag{22}$$

Once again, this can be written in matrix form as the following eigenvalue problem

$$\mathbf{A}\delta\mathbf{u}_0 = s\delta\mathbf{u}_0 \ , \tag{23}$$

with $\delta\mathbf{u}_0 = (\delta\rho_0, \delta p_0)^\top$ and

$$\mathbf{A} = \begin{bmatrix} -k^2\eta & ik \\ ik\kappa + \alpha_1 p_0 & -2\alpha_0 + ik\lambda p_0 - \mu k^2 \end{bmatrix} \tag{24}$$

We know that the stability conditions are given by the sign of $\mathrm{Re}[s]$; the eigenvalues of this 2×2 matrix are given by

$$s = \frac{\mathrm{Tr}\mathbf{A}}{2} \pm \frac{1}{2}\sqrt{(\mathrm{Tr}\mathbf{A})^2 - 4\det\mathbf{A}} \tag{25}$$

i.e.

$$s = \frac{1}{2}\Big[-2\alpha_0 + ik\lambda p_0 - k^2(\mu + \eta) \Big]$$
$$\pm \frac{1}{2}\Big[\big(-2\alpha_0 + ik\lambda p_0 - k^2(\mu + \eta)\big)^2 - 4(\kappa k^2 + 2\alpha_0\eta k^2 + \eta\mu k^4 - ik\alpha_1 p_0 - ik^3\lambda\eta p_0) \Big]^{1/2} \tag{26}$$

Assuming that the discriminant is positive, we can expand s to lowest order in k to obtain the following two eigenvalues in the hydrodynamic limit $(k \to 0)$

$$s_+ = -\frac{\big[8\alpha_0^3\eta - \alpha_1^2 p_0^2 + 4\alpha_0^2\kappa + 2\alpha_0\alpha_1\lambda p_0^2\big] k^2}{8\alpha_0^3} + i\frac{k\alpha_1 p_0}{2\alpha_0} + \mathcal{O}(k^3) \tag{27}$$

and

$$s_- = -2\alpha_0 + \frac{\big[4\alpha_0^2(\kappa - 2\alpha_0\mu) - \alpha_1^2 p_0^2 + 2\alpha_0\alpha_1 p_0^2\lambda\big] k^2}{8\alpha_0^3} + i\frac{kg_0}{2}\Big[2\lambda - \frac{\alpha_1}{\alpha_0}\Big] + \mathcal{O}(k^3) \tag{28}$$

Finally, at the lowest order in k, the real part of s is thus given by

$$\boxed{\mathrm{Re}[s] = \begin{cases} -2\alpha_0 + \mathcal{O}(k^2) \\ \frac{k^2}{8\alpha_0^2}\Big[\frac{\alpha_1^2}{\beta} - 2\alpha_0\Big[2\kappa + 4\eta\alpha_0 + \frac{\alpha_1\lambda}{\beta}\Big]\Big] + \mathcal{O}(k^3) \end{cases}} \tag{29}$$

We interpret these solutions as follows:

- the first eigenvalue $-2\alpha_0$ characterizes the *fast relaxation of the momentum fluctuations around the mean field value $p_0 = \sqrt{\alpha_0/\beta}$ in the absence of spatial variations $(k \to 0)$*;

- the second eigenvalue controls the *onset of instability of the homogeneous ordered phase*.

As long as $\alpha_0 > 0$, we have fast relaxation of the momentum fluctuations around the mean field value: the phase remains ordered. Instability leading to phase separation sets in when

$$\frac{\alpha_1^2}{\beta} - 2\alpha_0\Big[2\kappa + 4\eta\alpha_0 + \frac{\alpha_1\lambda}{\beta}\Big] > 0 \tag{30}$$

First, we find the roots of the associated quadratic equation: $\alpha_1^2 - 2\alpha_0\lambda\alpha_1 - 4\alpha_0\beta\kappa - 8\eta\alpha_0^2\beta = 0$. The discriminant of this quadratic equation is given by

$$\Delta = 4\alpha_0^2\lambda^2 + 16\alpha_0\kappa\beta + 32\eta\alpha_0\beta \tag{31}$$

The sign of the discriminant dictates the existence of real roots. As $\beta > 0$, if $\kappa < -[\alpha_0\lambda^2/4\beta + 2\eta]$, the quadratic equation does not have real solutions and the inequality is always met. This means that the *homogeneous state is thus always unstable*.

Conversely, if $\kappa > -[\alpha_0\lambda^2/4\beta + 2\eta]$, the roots of the quadratic equation are given by

$$\alpha_1 = \alpha_0\lambda \pm \sqrt{\alpha_0^2\lambda^2 + 4\alpha_0\kappa\beta + 8\eta\alpha_0\beta} \tag{32}$$

We conclude that if $\kappa > -[\alpha_0\lambda^2/4\beta + 2\eta]$, the instability sets in only when

$$\alpha_1 < \alpha_0\lambda\left[1 - \sqrt{1 + \frac{4(\kappa + 2\eta)\beta}{\alpha_0\lambda^2}}\right] \quad \text{or} \quad \alpha_1 > \alpha_0\lambda\left[1 + \sqrt{1 + \frac{4(\kappa + 2\eta)\beta}{\alpha_0\lambda^2}}\right] \tag{33}$$

Under these instability conditions, the homogeneous ordered phase is unstable. We will see in what follows that in this case, the instability can lead to the emergence of one of the three remaining phase co-existences: cO-dD (*banding*), cD-dO (*reverse banding*) or cO-dO (*comoving phases*). Interestingly, in the ordered phase, the homogeneous state can remain stable even if κ is negative, as long as the above stability conditions are satisfied.

II. PARTICULAR MODELS

A. A first example

In general, we are free to choose any functional form for $\alpha(\rho)$ and $\kappa(\rho)$. Here, we consider a specific model and use the previous results to study when this model can lead to non-trivial phase co-existence. We consider the following model

$$\alpha(\rho) = -A + \rho - \rho^2 \tag{34}$$

$$\kappa(\rho) = K - \frac{5}{6}\rho + \rho^2 \tag{35}$$

and $\lambda = \mu = \beta = \eta = 1$.

We have seen above that the condition for existence of collective motion is $\alpha(\rho) > 0$. In this model, α can become positive when the discriminant of the quadratic equation $\rho^2 - \rho + A = 0$ is positive, i.e. when $A < 1/4$. We conclude that collective motion is possible in this model when

$$\frac{1}{2}\left(1 - \sqrt{1 - 4A}\right) < \rho < \frac{1}{2}\left(1 + \sqrt{1 - 4A}\right) \tag{36}$$

In particular, within the region where $\alpha(\rho) < 0$, we can linearize the expression of α and write

$$\alpha(\rho) = (-A + \rho_0 - \rho_0^2) + (1 - 2\rho_0)\delta\rho + \mathcal{O}(\delta\rho^2) \tag{37}$$

where we have introduced $\rho = \rho_0 + \delta\rho$. Thus, identifying this expression to the results we derived in Section I B, we write $\alpha(\rho) = \alpha_0 + \alpha_1\delta\rho$ with

$$\alpha_0 = (-A + \rho_0 - \rho_0^2) \tag{38}$$

$$\alpha_1 = (1 - 2\rho_0) \tag{39}$$

Substituting this into Equation (30), we obtain the following condition

$$\frac{(1 - 2\rho_0)^2}{\beta} - 2(-A + \rho_0 - \rho_0^2)\left[2\left(K - \frac{5\rho_0}{6} + \rho_0^2\right) + 4\eta\left(-A + \rho_0 - \rho_0^2\right) + \frac{1 - 2\rho_0}{\beta}\right] > 0 \tag{40}$$

The locus corresponds to the roots of a quartic equations and the analytical expressions are not illuminating. However, the instability regions can be easily obtained numerically. Figure 1 summarizes the conditions for instability. In Figures 2 and 3, colored regions correspond to the colors in Figure 1, i.e.:

- **white region**, homogeneous disordered;

- **red region**, $\alpha_0 < 0$ and $\kappa_0 - \eta\alpha_0 < 0$ leading to a phase co-existence;

- **orange region**, $\alpha_0 > 0$ and $\kappa_0 < -[\alpha_0\lambda^2/4\beta + 2\eta]$ leading to a phase co-existence;

- **blue region**, $\alpha_0 > 0$ and $\kappa_0 > -[\alpha_0\lambda^2/4\beta + 2\eta]$ and $\alpha_1^2/\beta - 2\alpha_0[2\kappa_0 + 4\eta\alpha_0 + \alpha_1\lambda/\beta] > 0$ leading to a phase co-existence;

- **grey region**, $\alpha_0 > 0$ but no instability condition met leading to a homogeneous ordered phase.

Note that the color scheme used here refers to the parameter ranges that lead to instability, which is distinct from the color scheme used in Fig. 2 in the main text, which depicts the types of phase co-existence of the system.
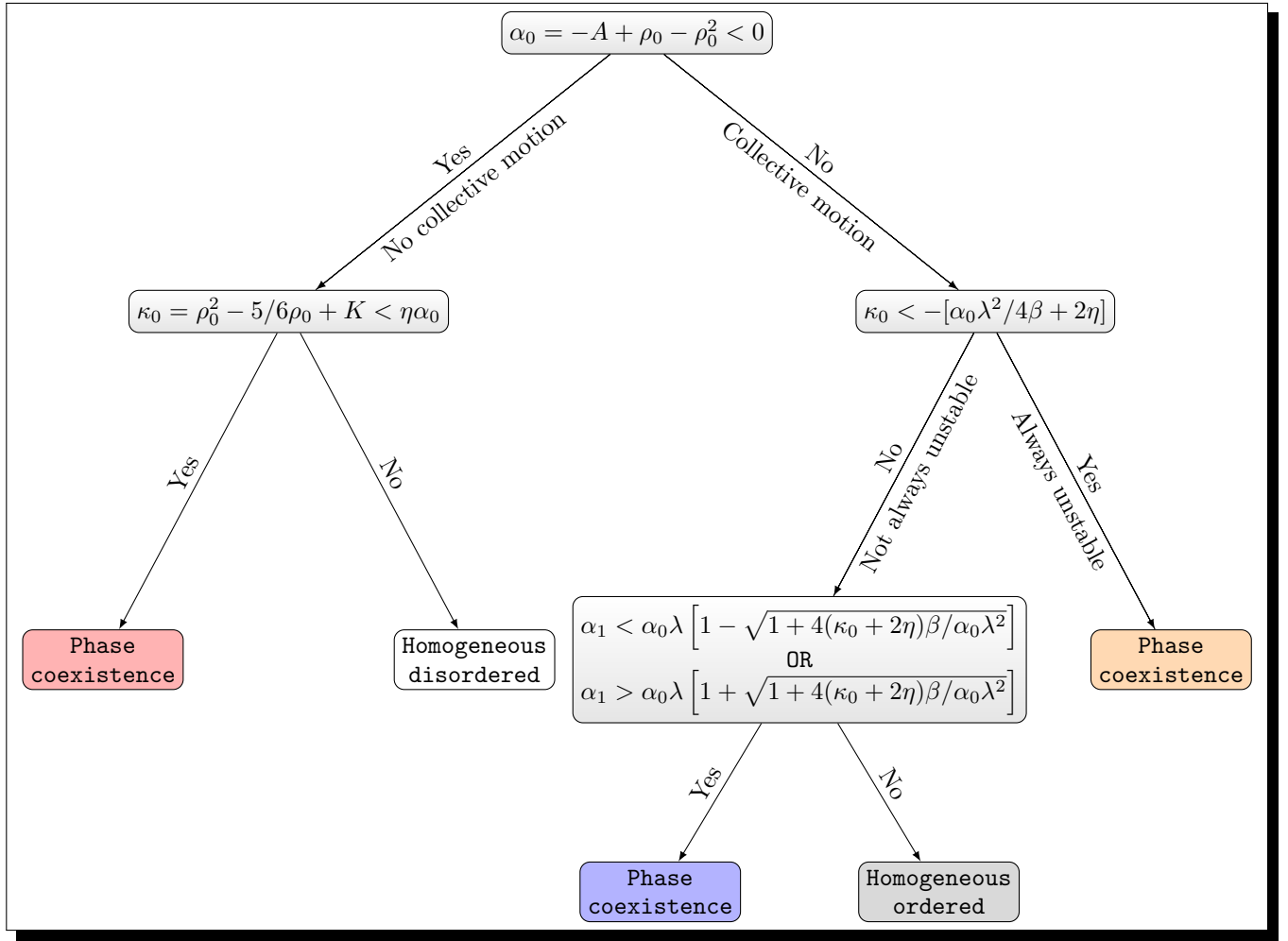
FIG. 1. Conditions for instability stemming from the linear stability analysis; the colorscheme used corresponds to the color of the instability regions in the phase diagrams.
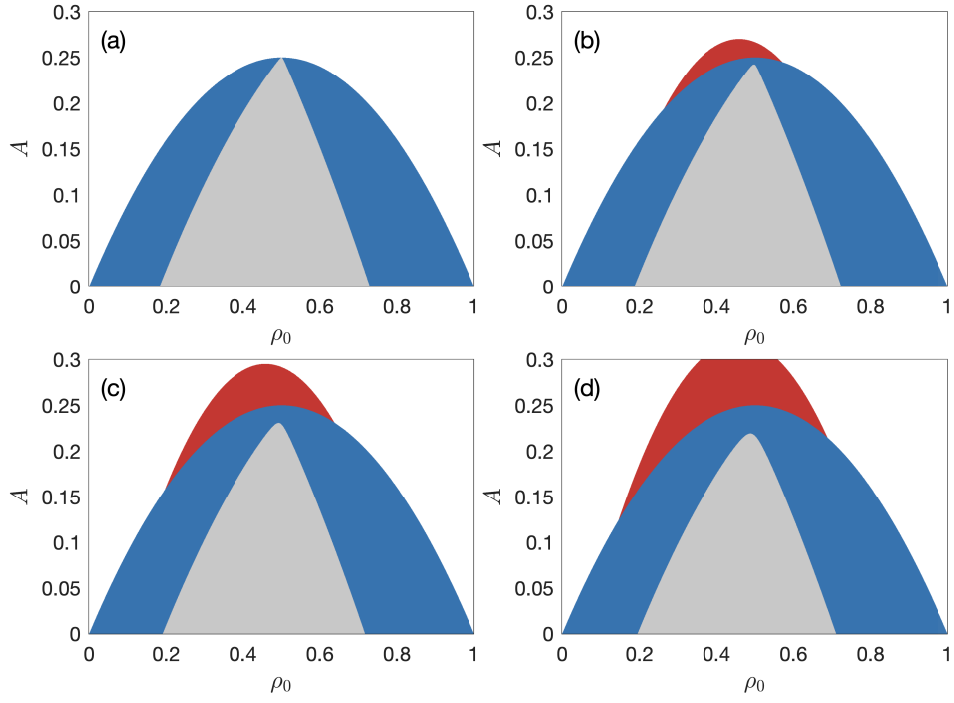
FIG. 2. Instability regions for the model defined by Eqs. (34) and (35) with fixed K with values (a) 0.175, (b) 0.15, (c) 0.125 and (d) 0.1.
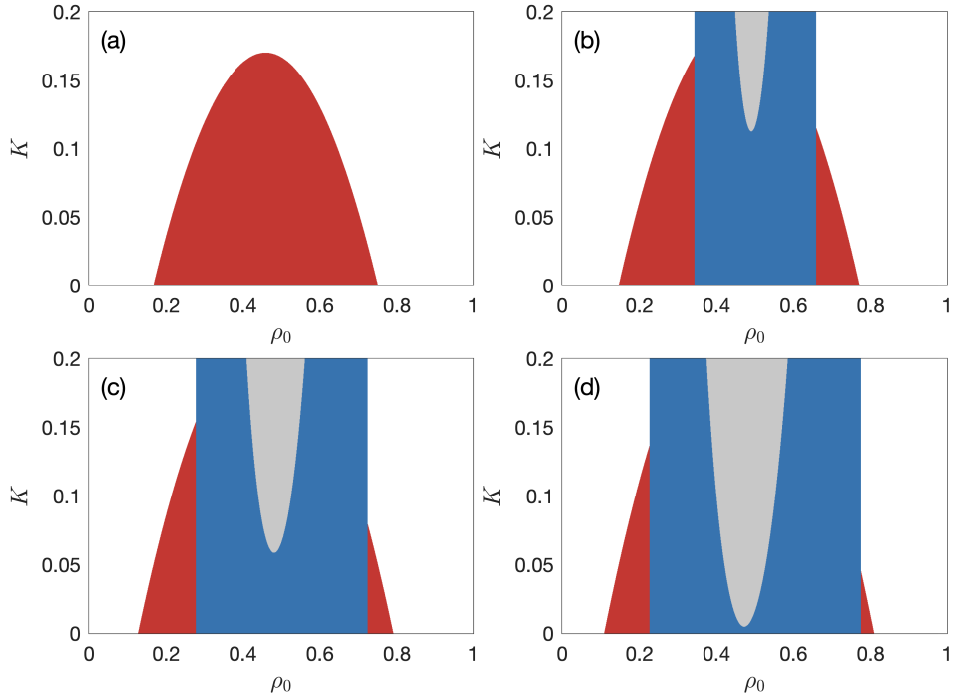

FIG. 3. Instability regions for the model defined by Eqs. (34) and (35) with fixed A with values (a) 0.25, (b) 0.225, (c) 0.2 and (d) 0.175.

B. Phase diagrams

Using the method outlined in the main text, we can construct qualitatively the corresponding phase diagrams given the instability regions. Briefly, the crucial ingredient here is that the instability regions is analogous to the spinodal decomposition region in thermal phase separation, which is always flanked by the nucleation and growth regions, which are metastable (and hence stable under linear stability analysis). Therefore, the phase separation boundaries (or the binodal lines) always extend further from the instability boundaries.

For instance, the corresponding phase diagrams of Fig. 2(a) and (c) are depicted qualitatively in Fig. 4, and those of Fig. 3(a) and (c) are shown in Fig. 5. In Figs. 4 and 5, all instability regions (obtained via our linear stability analysis) are shown as a shaded (grey) area while homogeneous regions are shown in white.
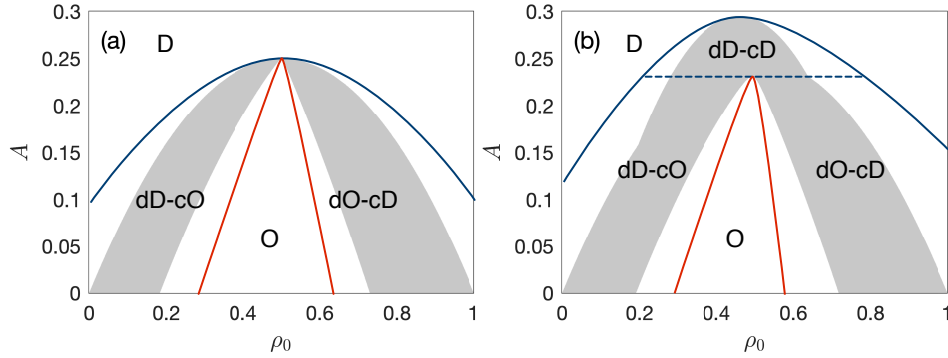

FIG. 4. Schematics of the phase diagrams of Fig. 2(a) and (c), respectively. The different homogeneous phases and phase co-existences are separated by the blue solid, blue broken, and red lines.
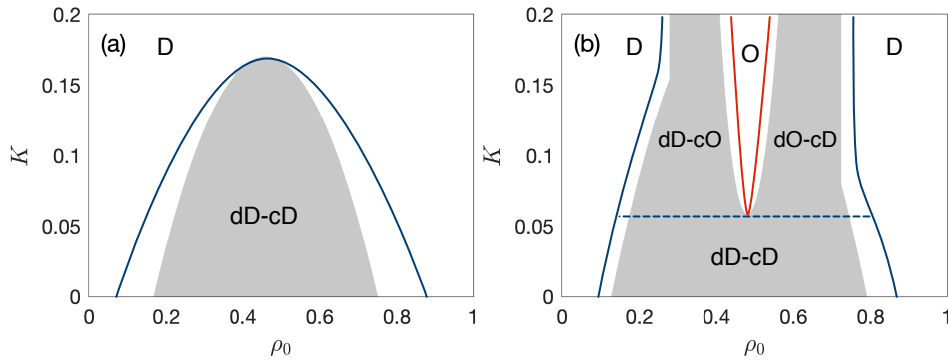

FIG. 5. Schematics of the phase diagrams of Fig. 3(a) and (c), respectively. The different homogeneous phases and phase co-existences are separated by the blue solid, blue broken, and red lines.

C. A model displaying the new comoving phase co-existence

We now discuss the model system discussed in the main text, in which

$$\alpha(\rho) = -A + 18\rho - 10/3\rho^2 \tag{41}$$
$$\kappa(\rho) = 140 - 145\rho + 30\rho^2 \ . \tag{42}$$

The instability regions are shown in Fig. 6 and the corresponding phase diagram is shown in Fig. 2 in the main text. In the next section, we provide details of the numerical methods that enables us to determine the various phase boundaries for this system.
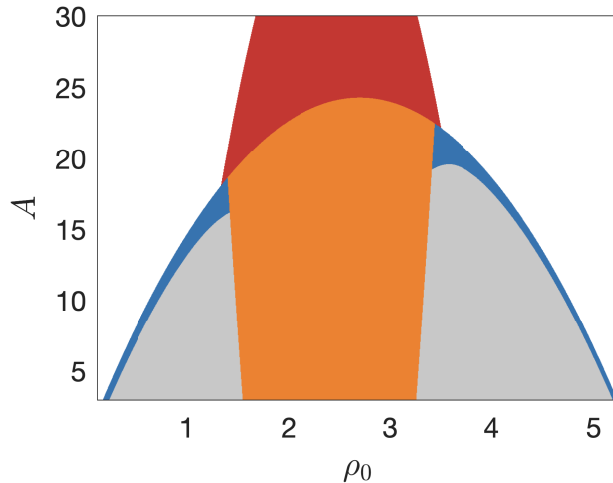
FIG. 6. Instability regions for the system of Equations (41–42) with diffusion term present in the EOM for ρ ($\eta = 2$) as in the main text.
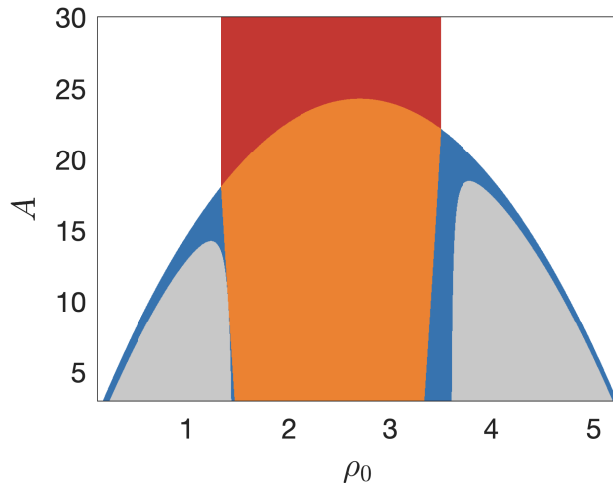

FIG. 7. Instability regions for the system of Equations (41–42) without diffusion term in the EOM for ρ ($\eta = 0$).

Finally, we also conduct our linear stability analysis in the case where the diffusion term is not present ($\eta = 0$). We show in Fig. 7 the diagram of instability regions. In particular, we find by comparing Figs. 6 and 7 that the shape of the instability regions is not qualitatively impacted by the absence of the diffusion term and we thus believe that our analysis applies generally to the case of $\eta = 0$ as well.

III.   NUMERICAL METHODS

The stationary profiles displayed in the main text are obtained via direct numerical integration of Eqs. (1) and (2). To do so, we discretize space using a linearly-spaced grid with spacing Δx and use a central finite difference approximation accurate to order $\mathcal{O}(\Delta x^8)$ for the spatial derivatives. The resulting set of ordinary differential equations is integrated using a variable order implicit scheme with adaptive time-stepping (ODE15s from MATLAB — `https://www.mathworks.com/help/matlab/ref/ode15s.html`).

The results of numerical simulations shown in the main text were obtained for a domain size $L = 100$ and $\Delta x \in [0.1, 0.2]$, with periodic boundary conditions. In all our simulations, we used the following parameters $\eta = 2$, $\lambda = 1$,

$\beta = 0.5$ and $\mu = 1$. We made sure to reach a stable steady-state in our simulations by simulating the system for at least a total time $T = 500$. To confirm the consistency of our results, we compared the steady-state profiles obtained for a variety of initial conditions (e.g., by varying the values of ρ_c, ρ_d, p_d, and p_c as described below). For the data shown in Fig. 1 and Fig. 2 of the main text, we used as initial conditions a double sigmoid with sharp interfaces:

$$\rho_1(x) = \rho_d + \frac{\rho_c - \rho_d}{1 + \exp\left[-(x - L/4)\right]}$$

$$\rho_2(x) = \rho_d + \frac{\rho_c - \rho_d}{1 + \exp\left[(x - 3L/4)\right]}$$

$$\rho(x, 0) = \min(\rho_1(x), \rho_2(x))$$

and if $p_c > p_d$,

$$p_1(x) = p_d + \frac{p_c - p_d}{1 + \exp\left[-(x - L/4)\right]}$$

$$p_2(x) = p_d + \frac{p_c - p_d}{1 + \exp\left[(x - 3L/4)\right]}$$

$$p(x, 0) = \min(p_1(x), p_2(x)) \ ,$$

while if $p_c < p_d$,

$$p_1(x) = p_c - \frac{p_c - p_d}{1 + \exp\left[-(x - L/4)\right]}$$

$$p_2(x) = p_c - \frac{p_c - p_d}{1 + \exp\left[(x - 3L/4)\right]}$$

$$p(x, 0) = \max\left(p_1(x), p_2(x)\right)$$

To produce the binodal lines in Fig. 2 of the main text, we varied A (by small increments of $\Delta A = 0.25$) and initialized the system with densities taken at the edges of the corresponding instability region. We summarize in the Table I the parameters used for the 6 profiles shown in Fig. 1 of the main text and the associated supplementary movies S1 to S6.

Supp. Movie	Phase co-existence	Fig. Panel	A	ρ_0	ρ_d	ρ_c	p_d	p_c
S1	**dD-cD**	Fig. 1(a)	24	2.5	1.5	3.5	0	0
S2	**dO-cO**	Fig. 1(b) (blue line)	7	2.5	1.0	4.0	1	2
S3	**dO-cO**	Fig. 1(b) (red line)	8	2.5	1.0	4.0	−1	1
S4	**dD-cO**	Fig. 1(c) (blue line)	7	0.45	0.4	0.5	0	1
S5	**dD-cO**	Fig. 1(c) (red line)	14.75	2.35	0.7	4.0	0	1
S6	**dO-cD**	Fig. 1(d)	14	4.45	4.4	4.5	0	−1

TABLE I. Simulation parameters (A, ρ_0) for steady-state profiles from Fig. 1 of the main text (and corresponding movies S1 to S6); we also include in the table the initial conditions parameters $(\rho_d, \rho_c, p_d, p_c)$.

IV. MULTICRITICAL POINT

At the linear level around the multi-critical point $(\kappa_0 = \kappa_1 = \alpha_0 = \alpha_1 = 0)$, the EOM are

$$\partial_t \delta\rho + \nabla \cdot \mathbf{p} = \eta \nabla^2 \delta\rho \quad , \quad \partial_t \mathbf{p} = \mu \nabla^2 \mathbf{p} + \mathbf{f} \ , \tag{43}$$

where $\mathbf{f}$ is a Gaussian noise term with a non-zero standard deviation.

Performing the following re-scalings:

$$\mathbf{r} \mapsto e^{\ell}\mathbf{r} \quad , \quad t \mapsto e^{z\ell}t \tag{44}$$

$$\delta\rho \mapsto e^{\chi_\rho \ell}\delta\rho \quad , \quad \mathbf{p} \mapsto e^{\chi_p \ell}\mathbf{p} \ , \tag{45}$$

the EOM become

$$e^{(\chi_\rho - z)\ell}\partial_t \delta\rho + e^{(\chi_p - 1)\ell}\nabla \cdot \mathbf{p} = e^{(\chi_\rho - 2)\ell}\eta\nabla^2 \delta\rho \quad , \quad e^{(\chi_p - z)\ell}\partial_t \mathbf{p} = e^{(\chi_p - 2)\ell}\mu\nabla^2 \mathbf{p} + e^{-(z+d)\ell/2}\mathbf{f} \ . \tag{46}$$

Therefore, the above linear EOM remain invariant if we make the following choice:

$$z = 2 \quad , \quad \chi_p = \frac{2-d}{2} \quad , \quad \chi_\rho = \frac{4-d}{2} \ . \tag{47}$$

Substituting these values into all possible nonlinear terms in the EOM of $\mathbf{p}$ (which is identical to the Toner-Tu equation), we find that as one decreases d from infinity, the first nonlinear term whose re-scaling based on the linear result diverges as $\ell \to \infty$ are $\delta\rho^2\mathbf{p}$ and $\nabla(\delta\rho^3)$. This is because, e.g., $\delta\rho^2\mathbf{p} \mapsto e^{((4-d)+(2-d)/2)\ell}\delta\rho^2\mathbf{p}$, and the exponent $(5 - 3d/2)\ell$ becomes greater than the re-scaling exponent of $\partial_t\mathbf{p}$, which is $(\chi_\rho - z)\ell = -(d+2)\ell/2$, at the upper critical dimension $d_c = 6$.